# Thermal and Crystallization Behaviors of Polyethylene Blends Synthesized by Binary Late Transition Metal Catalysts Combinations

**L. Pan,[1,2] Kun Y. Zhang,[1,2] Yan G. Li,[1,2] Shu Q. Bo,[1] Yue S. Li[1]**

[1]*State Key Laboratory of Polymer Physics and Chemistry, Changchun Institute of Applied Chemistry, Chinese Academy of Sciences, Changchun 130022, People's Republic of China*
[2]*Graduate School of the Chinese Academy of Sciences, Beijing 100049, People's Republic of China*

Received 24 June 2006; revised 16 November 2006; accepted 26 November 2006
DOI 10.1002/app.25960
Published online in Wiley InterScience (www.interscience.wiley.com).

**ABSTRACT:** A series of reactor blends of linear and branched polyethylenes have been prepared, in the presence of modified methylaluminoxane, using a combination of 2,6-bis[1-(2,6-dimethyphenylimino) pyridyl]-cobalt(II) dichloride (**1**), known as an active catalyst for producing linear polyethylene, and [1,4-bis(2,6-diidopropylphenyl)] acenaphthene diimine nickel(II) dibromide (**2**), which is active for the production of branched polyethylene. The polymerizations were performed at various levels of catalyst feed ratio at 10 bar. The linear correlation between catalyst activity and concentration of catalyst **2** suggested that the catalysts performed independently from each other. The weight-average molecular weights ($\overline{M}_w$), crystalline structures, and phase structures of the blends were investigated, using a combination of gel permeation chromatography, differential scanning calorimetry, wide-angle X-ray diffraction, and small angle X-ray scattering techniques. It was found that the polymerization activities and MWs and crystallization rate of the polymers took decreasing tendency with the increase of the catalyst **2** ratios, while melting temperatures ($T_m$), crystalline temperatures ($T_c$), and crystalline degrees took decreasing tendency. Long period was distinctly influenced by the amorphous component concentration.  J Appl Polym Sci 104: 4188–4198, 2007

**Key words:** blends; crystallization; polyethylene; synthesis

## INTRODUCTION

Polyolefin blends have been the subject of much research and development due to the excellent cost/performance balance of polyolefins in addition to the wide range of property gaps of individual polymers. For polyolefins, blending primarily aims at improving the balance of processability and mechanical properties of the final product. It is well known that both the molecular weight (MW) and microstructure of a polymer play a vital role in determining its physical and processing properties. The microstructural features of these polymers include the monomer and comonomer type, long chain branch length and distribution, comonomer content and comonomer distribution, MW, and molecular weight distribution (MWD). All of these structural features can be traced back to the original production of the polymers.[1–7] Recently, several studies have shown that ethylene polymerizations with the combination of different catalysts produce reactor blends with improved physical and/or chemical characteristics.[1,3,8–26] Nevertheless few of the ideal performances have been obtained.

The perfect polyolefin blends in industrial applications should own double peaks or broad MWD. Furthermore, the low MW component owns linear structure that provides rigidity, while the high MW component owns branched structure that provides flexibility. Basically, blending is achieved by four methods as below.[3–8,27–29] The first method involves the physical blending of polyolefin of two or more polymers with different MWs and microstructures to control the relative MWD. It is probably to obtain the ideal blends using this method, however, this widely used solution faces problems of energy consumption, operational cost, and miscibility limitation. The second method employs a series of reactors (tandem or cascade reactor systems), each one run under different polymerization reaction conditions, generating the desired bimodal MWD polymers with different MWs and microstructures. This method used at the pilot plant level has been revealed as expensive, cumbersome, and time-consuming. The third method utilizes the variation of operation conditions, such as temperature, comonomer concentration, and hydrogen

*Correspondence to:* Y. S. Li (ysli@ciac.jl.cn).
Contract grant sponsor: National Natural Science Foundation of China, SINOPEC; contract grant number: 20334030.
Contract grant sponsor: National Basic Research Program of China; contract grant number: 2005CB623801.

pressure, in a single reactor during polymerization. However, it is difficult for this method to obtain the ideal polymers because this method faces difficulties in controlling the MW and branched degree of the polymers, owing to the value of MW usually decrease with the increase of the branched degree. The fourth method is using two or more polymerization catalysts within a single reactor to produce polymers with different and controlled MWs, MWDs, and microstructures. In this method, each catalyst polymerizes ethylene independently, generating different polyethylenes during the polymerization reaction, and thus forming an ideal reactor blend. The simplicity of this method allows the polymer properties to be tailored by simple adjustment of the catalyst ratio and polymerization conditions. Considering the several families of olefin polymerization catalysts nowadays available will lead to polymers with specific microstructures, the composition of binary systems is extensive and the choice of the catalysts will be based on the polymer performances desired.

It is obvious that the choice of catalysts becomes the key to the designing of polyolefin's microstructures and characteristics. The ideal blends can be obtained when two proper catalyst, which can be used to synthesize low MW polymer with linear structure and high MW polymer with high branched individually are discovered. Lately, we have obtained a series of wide MWD polyethylene blends with lower MW, linear polyethylene (LPE), and higher MW, highly branched polyethylene (HBPE) by combination of catalysts in different feed ratio. Two late transition metal catalysts with different ratios were used: 2,6-Bis[1-(2,6-dimethyphenylimino) pyridyl] cobalt(II) dichloride (**1**), known as an active catalyst for producing LPE with low MW,[30–32] and [1,4-bis(2,6-diidopropylphenyl)] acenaphthene diimine nickel(II) dibromide (**2**), which is active for the production of high ($\overline{M}_w$), HBPE (Scheme 1).[29,32–35] The focus of this article is to investigate the effect of combining different ratio catalysts on blends' microstructures and to explore the possibility of using this technique to control the thermal and crystallinite characteristics of the products.

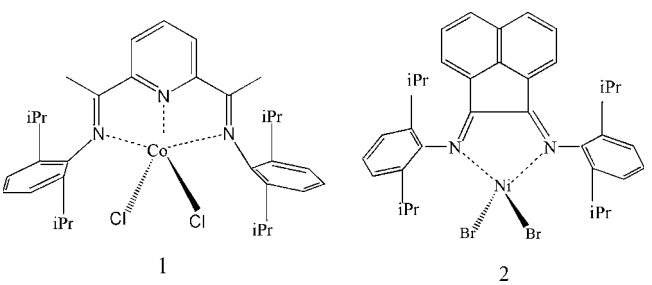


1 2

**Scheme 1** Structures of the two catalysts.

## EXPERIMENTAL

### Materials

Anhydrous toluene was purified by Solvent Purification System purchased from Mbraun. Modified methylaluminoxane (MMAO, 7% Aluminum in heptane solution) was purchased from Akzo Nobel Chemical. 2,6-Bis[1-(2,6-dimethyphenylimino) pyridyl]-cobalt(II) dichloride (**1**) and [1,4-bis(2,6-diidopropylphenyl)] acenaphthene diimine nickel(II) dibromide (**2**) were synthesized following the procedures reported in the literatures.[30–33]

### Typical polymerization procedure

High-pressure polymerization was carried out in a 1 L stainless steel reactor equipped with a mechanical stirrer and internal cooling water coils. The reactor was baked under nitrogen flow for 12 h at 150°C, subsequently cooled to the desired reaction temperature, and then purged by ethylene for 3 times. The prescribed amount of each catalyst (**1** and **2**) solution and toluene were injected simultaneously to the reactor via a gastight syringe. Ethylene was introduced into the reactor, and pressure was maintained at 10 atm throughout the polymerization run by continuously feeding ethylene gas. After proceeding for 60 min, the polymerization was stopped by turning the ethylene off and relieving the pressure. The reaction mixture was poured into a solution of HCl/ethanol (10 vol %). The polymer was isolated by filtration, washed with ethanol, and dried under vacuum at 60°C for 24 h.

### Characterization

The $\overline{M}_w$s and the MWDs of the samples were determined at 150°C by a PL-GPC 220 high-temperature gel permeation chromatograph equipped with three PL-gel 10 μm Mixed-BLS type columns, 1,2,4-Trichlorobenzene was employed as the solvent at a flow rate of 1.0 mL/min. The calibration was made by polystyrene standard EasiCal PS-1 (PL). The values of MW and MWD obtained by using polystyrene standard for these PE blends with different degree of branching were apparent data. The degree of branching of the branched polyethylene obtained from pure nickel complex was determined by quantitive $^{13}$C-NMR spectroscopy. The measurement was performed at 120°C on Varian Unity-400 using *o*-dichlorobenzene as solvent.

Differential scanning calorimetry (DSC) measurements were performed on a Perkin–Elmer Pyris 1 DSC instrument under $N_2$ atmosphere. The samples were heated from 0 to 150°C and cooled down to 0°C at a rate of 10°C/min. Melting temperature ($T_m$) and the value of fusion heat ($\Delta H_f$) were taken from the

**TABLE I**
**Ethylene Polymerization with Binary Catalytic System 1, 2/MMAO**

| Sample[a] | $X_2$[b] (%) | Activity[c] ($\times 10^{-5}$) | $\overline{M}_w$[d] (kg/mol) | MWD[d] | $Wt_{HBPE}$[e] (%) | $T_m$[f] (°C) | $T_c$[f] (°C) | $\Delta T_c$[g] (°C) | $\Delta H_m$[f] (J/g) | $X_c$[f] | $X_c$[h] |
|---|---|---|---|---|---|---|---|---|---|---|---|
| 1 | 0 | 16.37 | 22.87 | 3.03 | – | 133.1 | 120.8 | 12.3 | 200.0 | 0.79 | 0.82 |
| 2 | 12.50 | 16.83 | 111.55 | 10.36 | 21 | 132.1 | 119.3 | 12.8 | 147.8 | 0.73 | 0.65 |
| 3 | 16.67 | 17.22 | 147.13 | 8.29 | 30 | 131.2 | 118.2 | 13.0 | 128.8 | 0.72 | 0.59 |
| 4 | 20.00 | 18.12 | 155.78 | 8.62 | 35 | 130.8 | 117.5 | 13.4 | 122.6 | 0.70 | 0.53 |
| 5 | 29.41 | 19.01 | 172.41 | 9.76 | 47 | 130.7 | 116.9 | 13.8 | 85.0 | 0.60 | 0.42 |
| 6 | 33.33 | 19.53 | 187.08 | 8.11 | 59 | 129.0 | 113.2 | 15.8 | 58.9 | 0.55 | 0.29 |
| 7 | 50.00 | 19.85 | 217.87 | 8.65 | 68 | 126.0, 128.5 | 110.6 | 15.4, 17.9 | 38.9 | 0.46 | 0.24 |
| 8 | 58.33 | 20.72 | 239.49 | 7.18 | 75 | 126.5, 128.3 | 104.3 | 22.2, 24.0 | 4.9 | 0.07 | 0.12 |
| 9 | 100.0 | 21.58 | 252.42 | 2.80 | 100 | – | – | – | – | – | – |

[a] Synthesized at reaction conditions: solvent, and toluene; temperature, ambient temperature; Co + Ni = 60 μmol, Al/(Co + Ni) =1500 (molar).
[b] $X_2$ = moles of **2**/(moles of **2** + moles of **1**).
[c] Gram of PE/mol(Co + Ni).
[d] Determined by GPC.
[e] Weight content of the HBPE in the blends.
[f] Determined by DSC.
[g] $\Delta T_c = T_m - T_c$.
[h] Determined by WAXD.

second heating curve. The degree of crystallinity was calculated from $\Delta H_f$ using the eq. (1)[26]:

$$X_C^{DSC} = \Delta H_f / \Delta H_{f(STANDARD)} \quad (1)$$

The same instrument was utilized to study the isothermal crystallization kinetics of the blends. The samples were heated to 150°C and held for 3 min, then quickly cooled to the designed isothermal temperature, and then held for 30 min. The exothermic curves of heat flow as a function of time were recorded and investigated.

Wide-angle X-ray diffraction (WAXD) patterns were recorded in the reflection mode at room temperature using D/MAX 2500V, connected to a computer. The samples were pressed into 1 mm thick plates at 30–50°C above $T_m$s and then cooled to room temperature at 20°C/min. The diffraction scans were collected over a period of 20 min from 5° to 40° using a sampling rate of 1 Hz. The crystalline degrees ($W_{C,X}(X_C^{WAXD})$) of the PE blends were calculated via esq. (2) developed by Mo and Zhang.[36]

$$W_{C,X} = \frac{I_{110} + 1.42I_{200}}{I_{110} + 1.42I_{200} + 0.68I_a} \quad (2)$$

Small-angle X-ray scattering (SAXS) measurements were performed on the Philips PW-1700 Diffract meter connected with a Compact Kathy System, operated at 40 kV and 30 am with a 0.5° step size of 2θ from 0.08° to 3.0°. The samples were pressed into 1 mm thick plates at 30–50°C above $T_m$s and then cooled to room temperature at 20°C/min before tested. The absolute intensity for $I(S)$ has been evaluated using four slit collimation system, and the mensuration of absolute intensity has been carried out on standard samples.

## RESULTS AND DISCUSSION

### Choice of catalysts and effect of catalyst composition on the activity of polymerization

Just as we have illuminated in the introduction section, the choice of catalysts is the key to the designing of reactor blends' microstructures and characteristics. Therefore, we should find two proper catalysts, one can be used to synthesize low MW polymer with linear structure, and the other can be utilized to synthesize high MW polymer with high branched degree. Several catalyst systems have been chosen to synthesize PE blends,[1,3,8,12–22] however, few of ideal blends were obtained. It is well known that cationic (α-diimine nickel (II) catalyst produces high MW, polyethylene with changing branched structures depending on polymerization condition. Hence, Mecking chosen cationic α-diimine nickel and 2,6-bis(imino)pyridyl iron catalysts to synthesize reactor blends with different properties related to the PEs synthesized by catalysts separately,[1] Zhu reported a binary catalyst system containing metallocene ([rac-ethylenebis(indenyl) zirconium dichloride]) and Ni(α-diimine) $Br_2$.[5] However, the resulting blends display relatively narrow MWD but not double peaks or broad MWD because both cationic 2,6-bis(imino)pyridyl iron and *rac*-ethylenebis(indenyl) zirconium dichloride catalyst yield high MW polyethylene. Considering the fact that cationic 2,6-bis(imino)pyridyl cobalt catalyst yields LPEs with low MW under changing polymerization conditions, we choose 2,6-bis[1-(2,6-dimethyphenylimino)

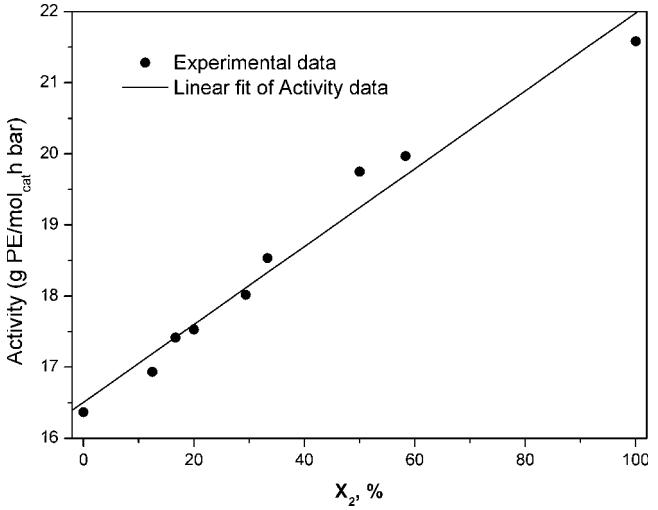


**Figure 1** Effect of the content of catalyst **2** on polymerization activities.

pyridyl]-cobalt(II) dichloride (**1**) and [1,4-bis(2,6-diidopropylphenyl)] acenaphthene diimine nickel(II) dibromide (**2**) to prepared the reactor PE blends which display real double peak distribution, namely, high MW component is high branched polyethylene and low MW component is linear polymer.

The ethylene polymerizations were carried out at different ratios of catalyst fractions at high ethylene pressure. Table I shows the results of ethylene polymerization reactions. As shown in this Table we can found that not only the polymerization activities, but also the MWs, MWDs, melt temperatures ($T_m$s), crystalline temperatures ($T_c$s), and crystalline degrees of the polyethylene blends varied with the catalyst **2** molar fraction ($X_2$).

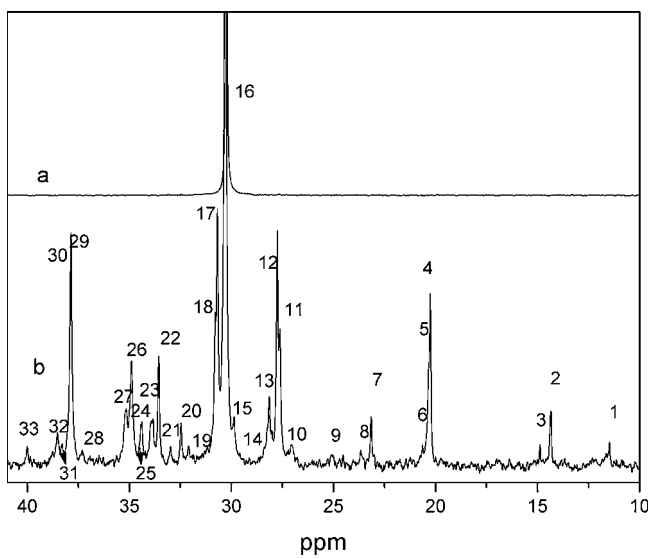


**Figure 2** $^{13}$C-NMR spectra of LPE (a) and HBPE (b) obtained from catalyst **1** and **2**, respectively.

**TABLE II**
**C$^{13}$-NMR Analysis of HBPE Synthesized from Catalyst 2**

| Entry | Branch content | Percentage over total branching | Percentage of branching | Total branching (%) |
|---|---|---|---|---|
| $N_{Methyl}$ | 5.733 | 38.68 | 11.76 | |
| $N_{Ethyl}$ | 1.394 | 9.41 | 2.86 | |
| $N_{Propyl}$ | 1.341 | 9.05 | 2.75 | ***30.43*** |
| $N_{Butyl}$ | 2.132 | 14.39 | 4.37 | |
| $N_{Amyl}$ | 1.137 | 7.67 | 2.33 | |
| $N_{Long(\geq 6)}$ | 3.093 | 20.87 | 6.35 | |

Figure 1 presents the relationship between polymerization activities and $X_2$. Under all the polymerization conditions, the catalyst **1**/MMAO system showed the lowest polymerization activity, while the catalyst **2**/MMAO system showed the highest activity. The polymerization activities increased linearly with the increases of $X_2$ in the reaction medium. This linear correlation between catalyst activity and $X_2$ suggested that the interactions between catalyst **1** and **2** species were minimal, and the catalysts performed independently from each other.

## Structures analysis

The branching degree analysis of Sample 1 and 9, obtained by single catalyst 1 or 2, was determined via quantitive $^{13}$C-NMR spectroscopy and shown in Figure 2. The chemical dislocations in the PE were calculated according to the rules of Galland and Quijada.[36–39] Table II gives the analysis result of branching degree of the HBPE. It is noteworthy that there are plenty of long branches ($n \geq 6$) presented besides the short branches (methyl, ethyl, butyl, amyl) in trace b (Sample 9), which is synthesized by catalyst **2**, while there is no side branch exiting in trace a (Sample 1). These long branches are confirmed by the presence of peak 20 and 15 at 32.47 and 29.86 ppm of trace b in Figure 2. Figure 3 displays how the different branches distributed in the main chain. It is very interesting

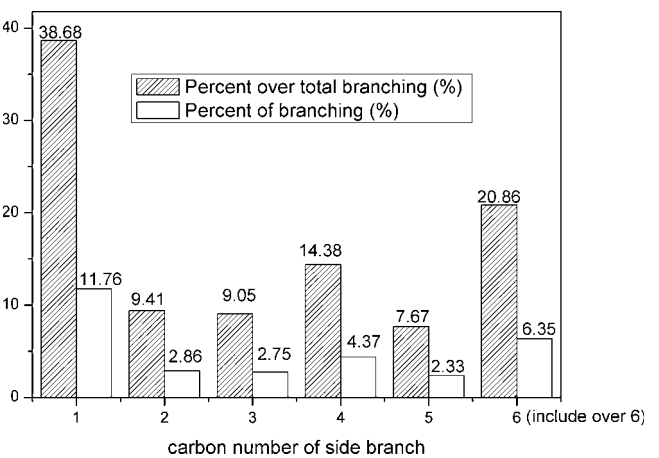


**Figure 3** Side chain distribution in the HBPE.

**TABLE III**
**The Analysis of Branching Degree of the Blends**

| Entry/sample | Branch degree[a] | Branch degree[b] |
|---|---|---|
| 1 | 0 | 0 |
| 2 | 0.0607 | 0.0619 |
| 3 | 0.0870 | 0.0913 |
| 4 | 0.1138 | 0.1065 |
| 5 | 0.1341 | 0.1430 |
| 6 | 0.1806 | 0.1795 |
| 7 | 0.1996 | 0.2029 |
| 8 | 0.2369 | 0.2282 |
| 9 | 0.3043 | 0.3043 |

[a] Determined by $C^{13}$-NMR measurements.
[b] Calculated data.

that the content of long branches is much more than the short chains except methyl. The calculated total branching degree of Sample 9 is up to 30.43%. Hereby, it is reasonable to suppose that the Sample 9 will show poor crystalline degree. The branching degrees of the PE blends were determined by quantitive $^{13}$C-NMR spectroscopy also. It is found that the result was nearly the same as the calculated data in Table III. The argument that the catalysts performed independently from each other was proved to be true.

The effect of $X_2$ on MW is given in Figure 4. As seen in the figure, there is a dependence of the $\overline{M}_w$ upon $X_2$. Higher $\overline{M}_w$ is observed for the blends by increasing $X_2$ in ethylene polymerization. Figure 5 presents MW distributions of some blends. In this picture, inhomogeneous double peaks with broad distribution can be seen from all PE blends, while the samples obtained by pure catalyst are typical single and narrow peaks. It is proved that these samples are well blended and it is an effective method to obtain broad distribution PE blends with different MWs and bimodal MW distributions by reactor blending with binary late transition metal catalysts combinations. The MWD of Sample 7 and the associated fit by a linear superposition of two Flory-Stockmayer distributions are presented at the top right of Figure 6. $A_1$ is area associated with LPE synthesized by catalyst **1** and $A_2$ is area associated with HBPE synthesized by catalyst **2**. Using this method, we can obtain all proportions of $A_1$ to $A_2$ ($A_1/A_2$) of all the PE blends. Moreover, the proportions of $A_1$ to $A_2$ are equal to the weight ratios of LPE to the weights of HBPE in the blends. Hence, the weight content of LPE ($Wt_{LPE}$) and the weight content of HBPE ($Wt_{HBPE}$) are obtained. The relationship between the weight ratios of LPE to HBPE and $X_2$ is shown in Figure 6. This relationship can be

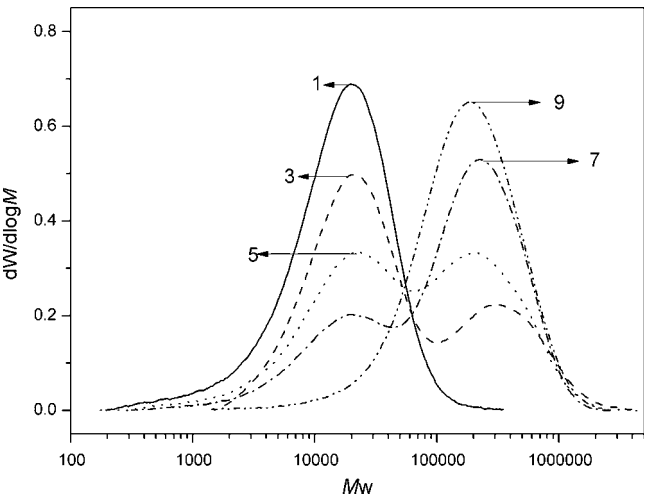


**Figure 5** Molecular weights distributions of the blends obtained by binary catalysts.

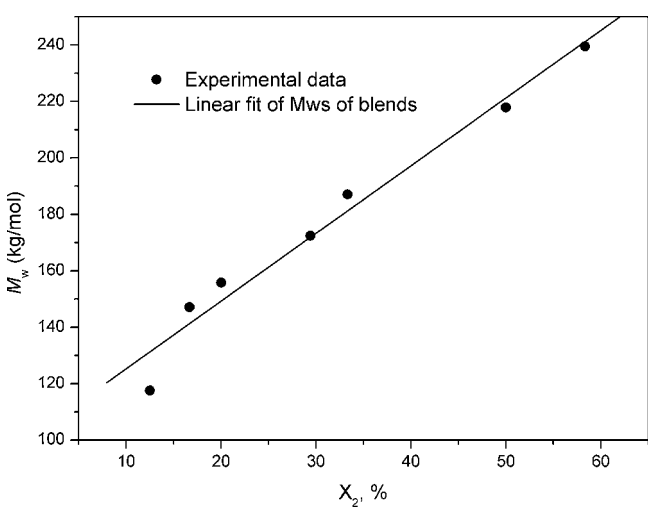


**Figure 4** Effect of the content of catalyst **2** on the molecular weights of the blends.

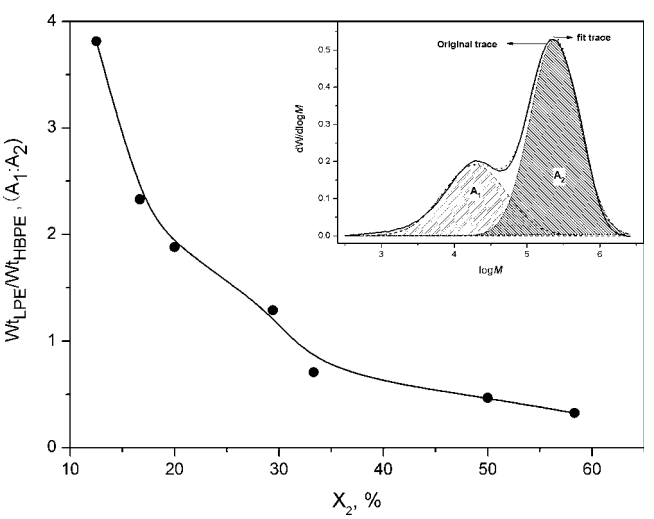


**Figure 6** Analyses of the weight ratios of LPE and HBPE in the blends and fit of bimodal MWD of Sample 7 with two Flory–Stockmayer distributions.

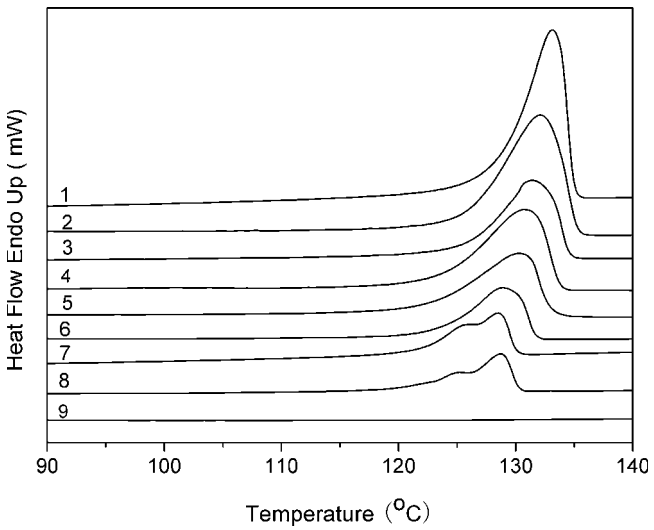


**Figure 7** Effect of the HBPE content on the $T_m$s of all PE samples.

guidance for designing PE blends with appropriate MW.

The results of DSC measurements of the PE samples obtained with the complexes **1** and **2** catalytic systems alone and with the mixtures obtained by these catalytic systems are shown in Figures 7 and 8. Because of the high degree of branching, no crystallization or melting peak is observed in the case of Sample 9, the HBPE. The amorphous structure of Sample 9 is proved again. Single crystallization and melting peaks were observed for Sample 1–6, while double melting endotherms were found for sample 7 and 8 in melting traces. The double melting behaviors of sample 7 and 8 may arise from the melting-recrystallization mechanism. Such behavior has also been observed and discussed earlier by others in similar systems.[36–40] It is shown that the increase of the HBPE content in the mixture of these catalytic systems causes the melting and crystallization peak profiles to shift towards low temperatures and become wider compared to those of the LPE obtained by catalyst **1**. The $T_m$ of the crystalline component in a polymer blend depends on both morphological and thermodynamic factors. The former is related to crystallization conditions (temperature, time, etc.), blend composition and scanning rate. These factors can cause an increase or a decrease of $T_m$. In the cases of miscible blends, the thermodynamic factor must be considered that whose contribution induces a decrease of $T_m$. Thus, when a crystalline component is miscible with an amorphous polymer, a depression of $T_m$ is observed.

The depression of crystallization temperature ($T_c$) in all samples may be ascribed to the two factors: first, as crystallization proceeds, there is a reduction of crystallizable polymer in the melt, and hence a concomitant decrease in the thermodynamic driving force, which is favoring crystallization. Second, as crystalline component is diluted with amorphous component, the transport process of crystalline component segments to the crystallite melt interface becomes more protracted, causing retardation in the rates of nucleation and growth of the crystal.[41]

Figure 9 shows the relationship between the crystalline degree and the HBPE content ($Wt_{HBPE}$) in the PE blends. It is noteworthy that the calculated line is not a straight line and not getting across the origin, indicating that the blends system are compatible and the adding of the amorphous component restrains the crystallization process of the crystalline LPE obtained by catalyst **1**.

Isothermal crystallizations were also carried out with the PE blends to assess the nature of the crystal-

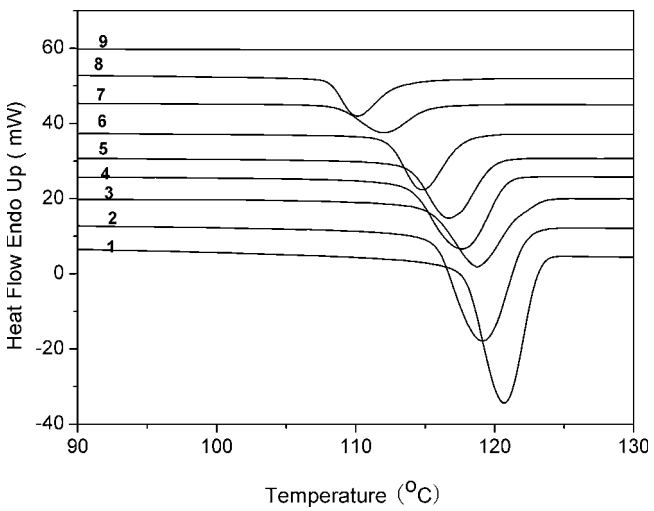


**Figure 8** Effect of the HBPE content on the $T_c$s of all PE samples.

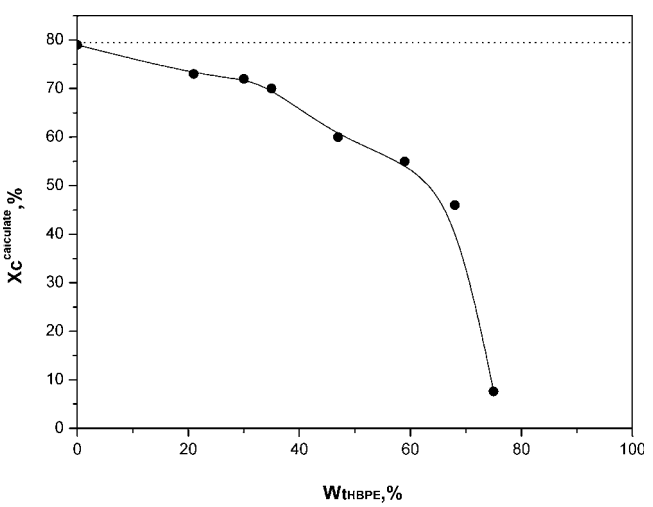


**Figure 9** Effect of the HBPE content on the crystallinity degrees of the blends.

lites developed. The blends were initially equilibrated in the melt at 150°C held for 3 min, and then rapidly cooled at the rate of 80°C/min, to the crystallization temperature ($T_c$) and maintained for 30 min. The bulk kinetics of isothermal crystallizations of blend was analyzed using the Avrami eq. (3)[42–55]:

$$\log[-\ln(1 - X_c)] = \log K + n \log t \quad (3)$$

Where $n$ is the Avrami exponent, which is related to the geometry of the spherical growth and the mechanism of the nucleation. $K$ is the overall kinetic rate constant. The time required to reach 50% crystallization is called half-time of crystallization and denoted as $t_{1/2}$ in eq. (4):

$$K = \ln\left(\frac{2}{t_{1/2}^n}\right) \quad (4)$$

Typical crystallization isotherms, obtained by plotting $X_c$ against time are shown in Figure 10 for Sample 7 at different crystallization temperatures. From such curves, the half-time of crystallization, $t_{1/2}$, can be deduced. It is obvious that the value of $t_{1/2}$ increased with the increase of temperature. As shown in Figure 11, all $t_{1/2}$ values increased with isothermal crystallization temperature and the rates of $t_{1/2}$ are very different for the PE blends with different HBPE content. It indicates that a decrease of crystallization rate at higher HBPE content and higher temperature, furthermore, the more amorphous component (HBPE) concentration, the more decrease of crystallization rate. Anyway, the thermal analysis shows that the addition of the amorphous component restrains the crystallization process of the crystalline LPE obviously.

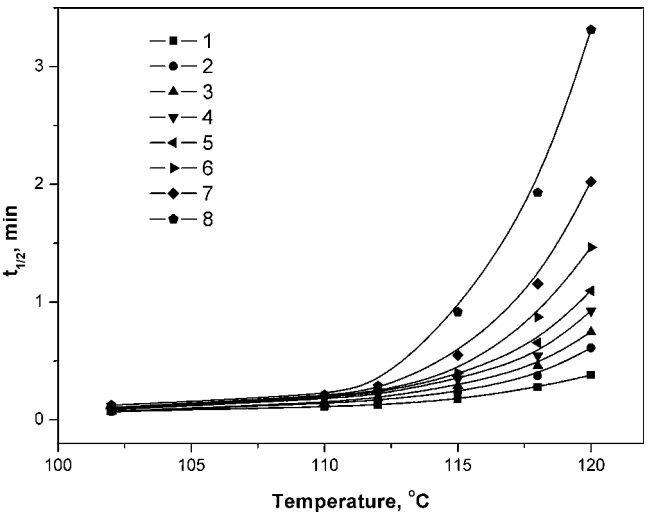


**Figure 11** Effects of HBPE content on the crystallization rate of the samples.

The studies on melting of a crystalline polymer blended with an amorphous one can give important information about miscibility and the polymer–polymer interactions. Thermodynamic considerations predict that the chemical potential of a polymer will be decreased by the addition of a miscible diluent. If the polymer is crystallizable, the decrease in chemical potential will result in a decrease of the equilibrium melting point. Figure 12 shows the plots of the $T_m$ versus $T_c$ of the samples with different HBPE content. As observed, good linear correlations between $T_m$ and $T_c$ of samples 1–5 (with lower amorphous component concentration) are obtained. The traces of these samples are parallel. According to the Hoffma–Weeks approach[56] the equilibrium melting point, $T_m^0$, could be determined by extrapolation of $T_m$ versus $T_c$ to $T_m$

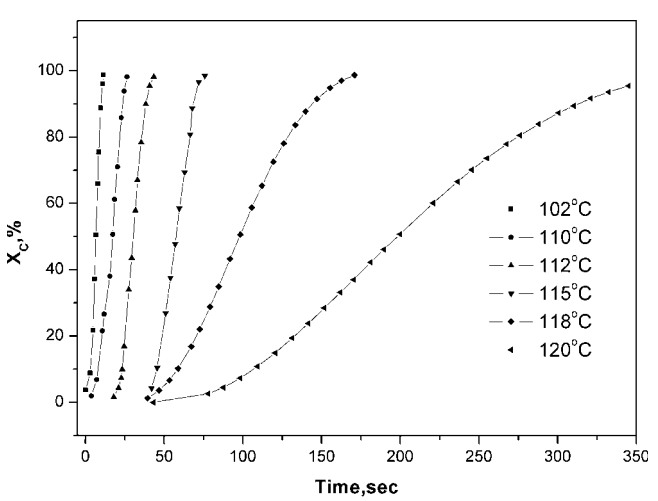


**Figure 10** Crystallization isotherms for the Sample 7 crystallized at different $T_c$.

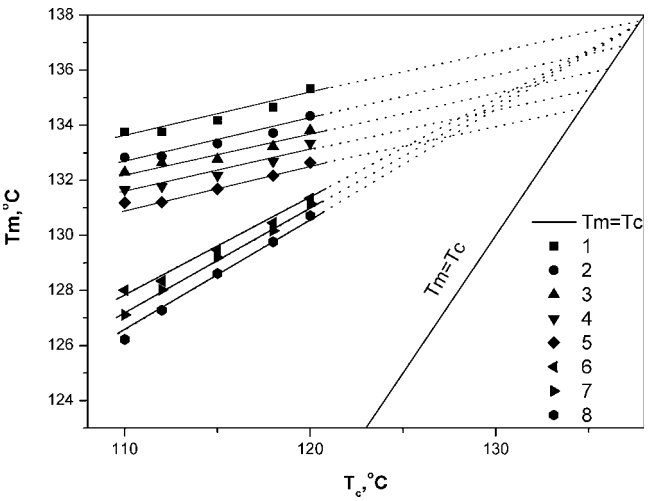


**Figure 12** Melting temperature versus the crystallization temperature for blends of different composition.

**TABLE IV**
**Equilibrium Melting Temperatures, $T_M^0$, and Stability Parameters, $\phi$, for Different Blend Compositions**

| Sample | $Wt_{HBPE}$ (%) | $^0_M$(K) | $\phi$ |
|---|---|---|---|
| 1 | – | 410.96 | 0.152 |
| 2 | 21 | 410.00 | 0.157 |
| 3 | 30 | 409.18 | 0.146 |
| 4 | 35 | 408.52 | 0.148 |
| 5 | 47 | 407.70 | 0.141 |
| 6 | 59 | 410.96 | 0.364 |
| 7 | 68 | 410.96 | 0.380 |
| 8 | 75 | 410.96 | 0.306 |

$= T_c$. The isothermal crystallization is described by the eq. (5):

$$T_m^0 - T_m = \phi(T_m^0 - T_c) \quad (5)$$

where $\phi$ is the stability parameter, which depends on the crystalline thickness. A fit of the data shown in Figure 12 yields the $T_m^0$ values, which are summarized in Table IV. It should be noted that the values of $\phi$ are between 0 and 1; $\phi = 0$ implies $T_m = T_m^0$ with the most stable crystals, and $\phi = 1$ implies $T_m = T_c$ with inherently unstable crystals. Therefore the $\phi$ values obtained for all the blends indicate that the crystals corresponding to the blends with lower HBPE content are fairly stable.

However, the behaviors of the sample 6, 7, 8 endotherms are quite different from samples 1∼5, as illustrated in Figure 12. The slopes of traces of the $T_m \sim T_c$ of the sample 6, 7, and 8 with higher HBPE content are also different, these three traces are intersect with the trace of $T_m = T_c$ at the same point and form a uniform balance while the $T_c$ is elevated. The values of $\phi$ parameter of these samples are about 0.4, indicating lower stability of the crystals than those of the former PE samples. It should be noted that the both lines, corresponding to sample 1 and the blends, extrapolate to the same $T_m^0$ value. This proves that the melting depression of the blends with higher HBPE content does not arise from thermodynamic effects and seems to be determined only by the decrease of the thickness of the crystalline lamellae of the sample i.e., the morphological effects, whereas the blends with lower HBPE content undergoes mainly a thermodynamic melting point depression. Furthermore, it is assumed that the existing of these two different factors (thermodynamic effects for the low HBPE content blends and morphological effects for the little higher HBPE content blends) results in the sudden jump of the $\phi$ parameter between the two set blends.

PE, under usual conditions, crystallizes in the typical orthorhombic lattice. It is evident that for all samples, the diffractograms exhibit major characteristic crystalline peaks of PE at scattering angles $2\theta = 21.46^\circ \pm 0.10^\circ$ and $23.70^\circ \pm 0.10^\circ$, which correspond to the reflection planes at 110 and 200, respectively. In this present study, the purpose of the WAXD experiment is to investigate whether or not the addition of amorphous HBPE affect the formation of crystals during crystallization and the amount of crystalline content formed. Figure 13 displays the different X-ray diffraction patterns found at room temperature for all the samples analyzed. It is clear that the peak positions from the WAXD profiles are almost identical, indicating the LPE chains form a similar unit-cell structure for the blends studied here. The intensities of the crystalline peaks of PE in blends decrease with the HBPE content increases.

As the HBPE content increases, the average number of consecutive ethylene units decreases and the crystallizable component becomes smaller. Consequently, the degree of crystallinity decreases while amorphous and interfacial content increase. This illuminates that with the addition of HBPE, the characteristic orthorhombic crystals are retained, i.e., the intrinsic crystalline structure of LPE (Sample 1) has not been influenced. The $X_C^{WAXD}$ values of the PE blends were calculated via eq. (2) and all results were listed in Table I. It is apparent that the increase of HBPE content leads to a considerable decrease of crystallinities in the blends.

Figure 14(a,b) presents the Lorentz-corrected SAXS profiles in absolute intensity unit obtained on the same set of samples used the in WAXD measurement. With a two-phase system comprising crystalline and amorphous fractions with distinct interface, the mean long period of the lamellar morphology could be estimated from the maximum value of the scattering vec-

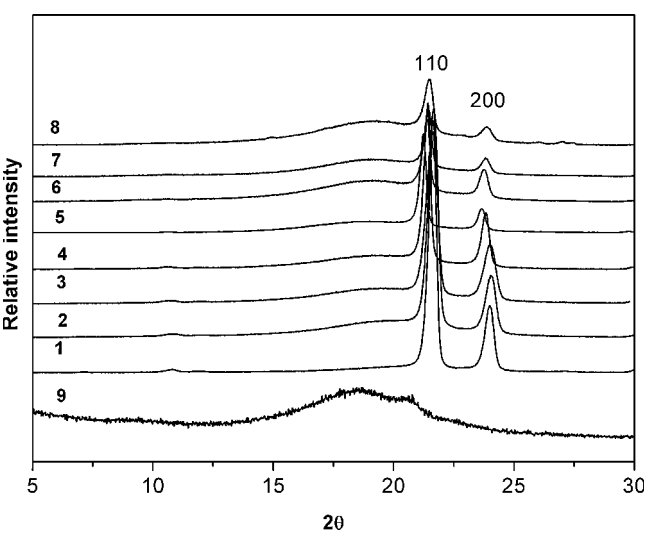


**Figure 13** X-ray diffractograms of all the PE samples.

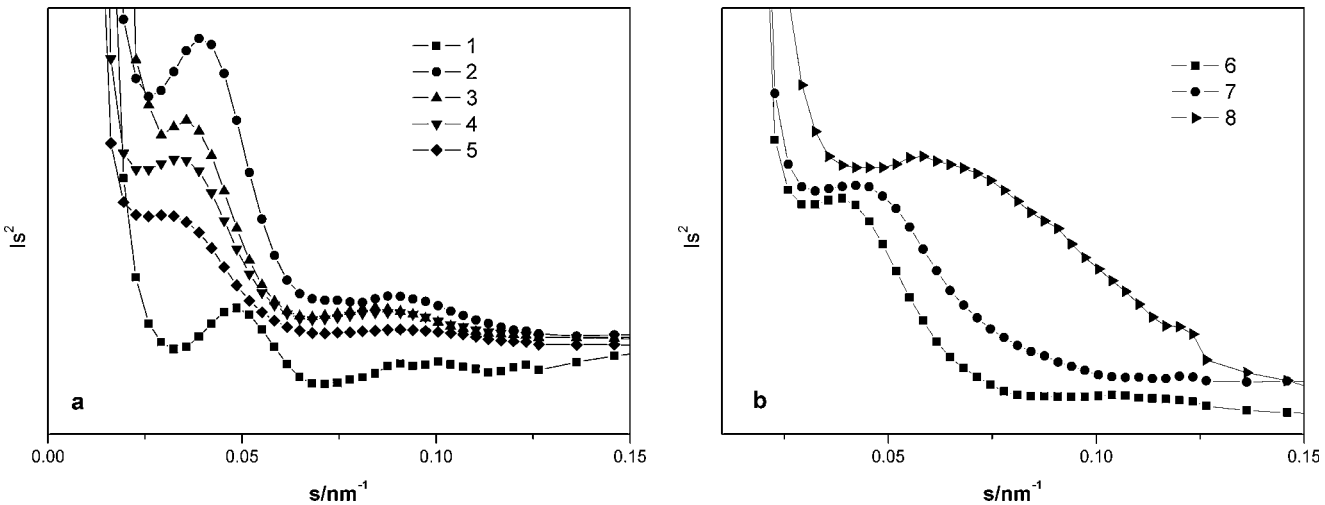


**Figure 14** (a,b) The Lorentz-corrected SAXS profiles of the PE blends.

tor $q_{max}$ observed in the Lorentz-corrected SAXS scattering profiles. The observed two reflection peaks in Figure 14(a) where the peak position ratios are almost 1:2 are the first and second order reflection corresponding to the lamellar structure.

On the basis of Bragg's law and the mathematical definition of the scattering vector $q$, the long period $L_B$ can be calculated from the following eqs. (6) and (7)[57,58]:

$$L_B = \frac{2\pi}{q_{max}} \tag{6}$$

$$q = \frac{4\pi \sin(\theta/2)}{\lambda} \tag{7}$$

It is assumed that the $L_B$ is composed by crystal region ($L_C$) and amorphous region ($L_A$) by arranged in an alternating fashion. The corresponding thickness of the crystalline region ($L_C$) can be calculated by the following eq. (8)

$$L_C = L_B X_C^{WAXD} \tag{8}$$

The $L_B$ and $L_C$ values calculated are listed in Table V. It is well known that the $L_B$ reflects the changes in densities for the crystalline and amorphous regions of polymers. As indicated in Table V and Figure 15, the $L_C$ values take on gradually decreasing tendency as HBPE content increases. It is notable that the $L_B$ values of the blends take on gradually increasing tendency until reach the maximum value at 34.27 nm. Here, we can suppose that the changes of $L_B$ values are dependent on the addition of amorphous component. At lower amorphous PE concentration ($Wt_{HBPE} \leq 47\%$), the additional LBPE can syncretize with the original amorphous region and there is little effect on the $L_C$, while the $L_A$ is increased as the HBPE increases. Thereby, the $L_B$ values take on increasing tendency. However, at higher amorphous PE concentration ($Wt_{HBPE} \geq 59\%$), the existence of abundant amorphous region has obvious effect on the $L_C$, making $L_C$'s value remarkably decreased, the crystalline

**TABLE V**
**Effect of HBPE Content ($Wt_{HBPE}$) on Crystalline Structure of PE Blends**

| Entry | 1 | 2 | 3 | 4 | 5 | 6 | 7 | 8 |
|---|---|---|---|---|---|---|---|---|
| $Wt_{HBPE}$ | 0 | 0.21 | 0.30 | 0.35 | 0.47 | 0.59 | 0.68 | 0.75 |
| $X_c^{WAXD}$ | 0.82 | 0.65 | 0.59 | 0.53 | 0.42 | 0.29 | 0.24 | 0.12 |
| $L_B$ (nm) | 20.58 | 25.71 | 28.03 | 30.78 | 34.27 | 25.70 | 23.72 | 17.08 |
| $L_C$ (nm) | 16.87 | 16.69 | 16.54 | 16.31 | 14.37 | 7.45 | 5.69 | 2.05 |

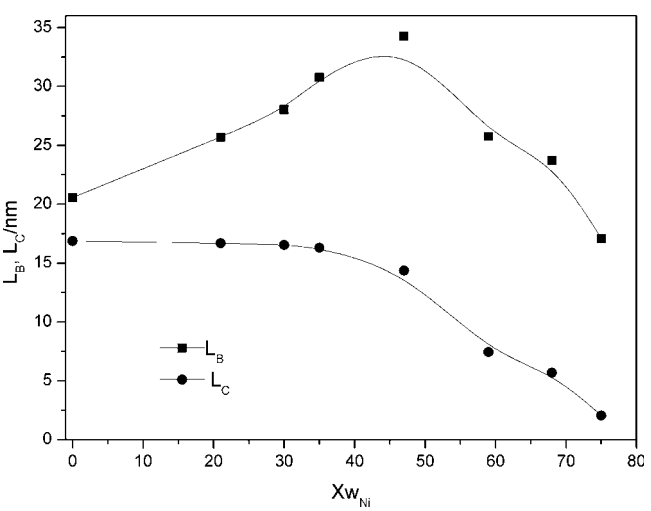


**Figure 15** Effect of HBPE content in the blends on the values of $L_B$ and $L_C$.

region and amorphous region are inclined to rearrange after been destroyed. As a result, the $L_B$ values take on decreasing tendency at higher HBPE concentration. Nevertheless, one thing should be illuminated here that the heat history of the entire samples tested by DSC and SAXS were not the same. The values of $L_C$ of sample 7 and 8 were fairly low compared with their melting points ($T_m$s). It could be ascribed that the crystalline rate of the samples with large quantity of amorphous components decreased so much that they couldnot crystallinize perfectly when cooled down at a rate of 20°C/min. As a result, the tested values of $L_B$ and $L_C$ might be lower than the actual values.

## CONCLUSIONS

A series of reactor blends of LPE and HBPE were prepared using a combination of 2,6-Bis[1-(2,6-dimethyphenylimino) pyridyl]-cobalt(II) dichloride (**1**)/MMAO and [1,4-bis(2,6-diidopropylphenyl)] acenaphthene diimine nickel(II) dibromide (**2**)/MMAO. The polymerization activities and apparent MWs of the blends increased with the increase of the catalyst **2** molar fractions ($X_2$). It was found that the melting temperatures, crystalline temperatures and crystalline degrees took decreasing tendency with the increase of HBPE content ($Wt_{\mathrm{HBPE}}$) in the blends. The isothermal analyses indicate that at lower $Wt_{\mathrm{HBPE}}$, the crystalline component is diluted by the addition of amorphous PE; and at higher $Wt_{\mathrm{HBPE}}$, the addition of amorphous component conduces disfigurement in the crystalline component or decrease the thickness of the lamellar crystallities. The $t_{1/2}$ values increased with the increase of isothermal crystallization temperature and HBPE content, indicating a decreased crystallization rate at higher temperature and higher amorphous component concentration. The SAXS analysis proved that the $L_B$ was distinctly influenced by the $Wt_{\mathrm{HBPE}}$. When $Wt_{\mathrm{HBPE}} \leq 47\%$, the amorphous region ($L_A$) was increased as the $Wt_{\mathrm{HBPE}}$ increasing, thereby, the $L_B$ values take on increasing tendency. When $Wt_{\mathrm{HBPE}} \geq 59\%$, and the existence of abundant amorphous region made $L_C$'s value remarkably decreased, and thus the crystalline region and amorphous region are destroyed and rearrange. As a result, the $L_B$ values took on decreasing tendency at higher amorphous PE concentration.

## References


1. Mecking, S. Macromol Rapid Commun 1999, 20, 139.
2. Shan, C. L. P.; Soares, J. B. P.; Penlidis, A. Polymer 2002, 43, 7345.
3. de Souza, R. F., Jr.; Casagrande, O. L. Macromol Rapid Commun 2001, 22, 1293.
4. Müller, A. J.; Arnal, M. L.; Spinelli, A. L.; Ca[icirc]nizales, E.; Puig, C. C.; Wang, H.; Han, C. C. Macromol Chem Phys 2003, 204, 1497.
5. Shimizu, K.; Wang, H.; Wang, Z. G.; Matsuba, G.; Kim, H.; Han, C. C. Polymer 2004, 45, 7061.
6. Matsuba, G.; Shimizu, K.; Wang, H. Z.; Wang, G.; Han, C. C. Polymer 2004, 45, 5137.
7. Wang, Z. G.; Wang, H.; Shimizuc, K.; Dong, J. Y.; Hsiaod, B. S.; Han, C. C. Polymer 2005, 46, 2675.
8. Alobaidi, F.; Zhu, S. P. J Appl Polym Sci 2005, 96, 2212.
9. Wu, T.; Li, Y.; Wu, G. Polymer 2005, 46, 3472.
10. Shan, C. L. P.; Soares, J. B. P.; Penlidis, A. Polymer 2003, 44, 177.
11. Tanem, B. S.; Stori, A. Polymer 2001, 42, 5389.
12. Kunrath, F. A.; Souza, R. F. D., Jr.; Casagrande, O. L. Macromol Rapid Commun 2000, 21, 277.
13. Han, T. K.; Choi, H. K.; Jeung, D. W.; Ko, Y. S.; Woo, S. I. Macromol Chem Phys 1995, 196, 2637.
14. D'agnillo, L.; Soares, J. B. P.; Penlidies, A. J Polym Sci Part A: Polym Chem 1998, 36, 831.
15. Komon, K. J. A.; Bazan, G. C. Macromol rapid commun 2001, 22, 467.
16. Beigzadeh, D.; Soares, J. B. P.; Duever, T. A.; Macromol Rapid Commun 1999, 20, 541.
17. Beigzadeh, D.; Soares, J. B. P.; Hamielec, A. H. J Appl Polym Sci 1999, 71, 1753.
18. Komon, K. J. A.; Bu, X.; Bazan, G. C. J Am Chem Soc 2000, 122, 1830.
19. de Souza, R. F.; Mauler, R. S.; Simon, L. C.; Nunes, F. F.; Vescia, D. V. S.; Cavajnolli, A. Macromol Rapid Commun 1997, 18, 795.
20. Gil, M. P.; dos Santos, J. H. Z., Jr.; Casagrande, O. L. Macromol Chem Phys 2001, 202, 319.
21. Mota, F. F.; dos Santos, R. M.; de Souza, R. F., Jr.; Casagrande, O. L. Macromol Chem Phys 2001, 202, 1016.
22. Quijada, R.; Rojas, R.; Bazan, G.; Komon, Z. J. A.; Mauler, R. S.; Ganlland, G. B. Macromolecules 2001, 34, 2411.
23. Quijada, R.; Narvaez, A.; Rojas, R.; Rabagliati, F. M.; Galland, G. B.; Mauler, R. S.; Benabente, R.; Perez, E.; Prere[tilde]na, J.; Bello, A. Macromol Chem Phys 1999, 200, 1306.
24. Chien, J. C. W.; Iwamoyo, Y.; Rausch, M. D.; Wedler, W.; Winter, H. H. Macromolecules 1997, 30, 3447.
25. Chien, J. C. W.; Iwamoyo, Y.; Rausch, M. D. J Polym Sci Part A: Polym Chem 2000, 37, 24395.
26. Yin, J. H.; Mo, Z. S. Modern Polymer Physics; Science Press: Beijing, 2001 (in Chinese).
27. Munoz-Escalona, A.; Lafuente, P.; Vega, J. F.; Munoz, M. E.; Santamaria, A. Polymer 1997, 38, 589.
28. Ahn, T. O.; Hong, S. C.; Kim, J.; Lee, H. D. J Appl Polym Sci 1998, 67, 2213.
29. Ittel, S. D.; Johnston, L. K.; Brookhart, M. Chem Rev 2000, 100, 1169.
30. Small, B. L.; Brookhart, M.; Bennett, A. M. A. J Am Chem Soc 1998, 120, 4049.
31. Britovsek, G. J. P.; Bruce, M.; Gibson, V. C.; Kimberley, B. S.; Maddox, P. J.; Mastroianni, S.; McTavish, S. J. P.; Redshaw, C.; Solan, G. A.; Strömberg, S.; White, A. J. P.; Williams, D. J. J Am Chem Soc 1999, 121, 8728.
32. Johnson, L. K.; Killian, C. M.; Brookhart, M. J Am Chem Soc 1995, 117, 6414.
33. Gates, D. P.; Svejda, S. A.; Õnate, E.; Killian, C. M.; Johnson, L. K.; White, P. S.; Brookhart, M. Macromolecules 2000, 33, 2320.
34. Zou, H.; Zhu, F. M.; Wu, Q.; Ai, J. Y.; Lin, S. A. J Polym Sci Part A: Polym Chem 2005, 43, 1325.
35. Jenkins, J. C.; Brookhart, M. J Am Chem Soc 2004, 126, 5827.
36. Mo, Z. S.; Zhang, H. F. Macromol Chem Phys C 1995, 35, 555.
37. Qiujada, R.; Dupont, J.; Correa, D. Macromol Rapid Commun 1995, 16, 357.

38. Soga, K.; Uozumi, T. Makromol Chem 1992, 193, 823.
39. Gallend, G. B.; de Souza, R. F.; Mauler, R. S.; Nunes, F. F. Macromolecules 1999, 32, 1620.
40. Michalak, A.; Ziegler, T. Macromolecules 2003, 36, 928.
41. Nishi, T.; Wang, T. T. Macromolecules 1975, 8, 909.
42. Avrami, M. J. J Chem Phys 1939, 7, 1103.
43. Avrami, M. J. J Chem Phys 1940, 8, 212.
44. Avrami, M. J. J Chem Phys 1941, 9, 177.
45. Wang, C.; Lin, C. C.; Tseng, L. C. Polymer 2006, 47, 390.
46. Sengupta, P.; Noordermeer, J. W. M. Polymer 2005, 46, 12298.
47. Pereira, R. P.; Rocco, O. A.; Maria, A. Polymer 2005, 46, 12493.
48. Liu, T. Y.; Lin, W. C.; Yang, M. C.; Chen, S.Y. Polymer 2005, 46, 12586.
49. Kuo, S. W.; Huang, C. F.; Tung, P. H.; Huang, W. J.; Huang, J. M.; Chang, F. C Polymer 2005, 46, 9348.
50. Huang, J. M.; Yang, S. J. Polymer 2005, 46, 8068.
51. Laredo, E.; Grimau, M.; Barriola, P.; Bello, A.; Müller, A. J. Polymer 2005, 46, 6532.
52. Schuman, T.; Stepanov, E. V.; Nazarenko, S.; Capaccio, G.; Hiltner, A.; Baer, E. Macromolecules 1998, 31, 4551.
53. Chen, J. L.; Sun, Q.; Zou, Y. K.; Xue, G. Polymer 2002, 43, 6887.
54. Krumme, A.; Lehtinen, A.; Viikna, A. Polymer 2004, 40, 359.
55. Krumme, A.; Lehtinen, A.; Viikna, A. Polymer 2004, 40, 371.
56. Hoffman, J. D.; Weeks, J. J. J Res Natl Bur Std 1962, 66A, 13.
57. Wang, Z. G.; Hsiao, B. S.; Sirota, E. B.; Srinivas, S.; Polymer 2000, 41, 8825.